Available online at www.sciencedirect.com
ScienceDirect
Journal of Power Sources 164 (2007) 953–958
JOURNAL OF POWER SOURCES
www.elsevier.com/locate/jpowsour

Short communication

# Electrodeposition of mesoporous manganese dioxide supercapacitor electrodes through self-assembled triblock copolymer templates

Tong Xue [a], Cai-Ling Xu [a], Dan-Dan Zhao [a], Xiao-Hong Li [c], Hu-Lin Li [a,b,*]

[a] College of Chemistry and Chemical Engineering of Lanzhou University, Lanzhou, Gansu 730000, PR China
[b] College of Material Science and Engineering of Nanjing University of Aeronautics and Astronautics, Nanjing, Jiangsu 210016, PR China
[c] Department of Chemistry, University of Southampton, Southampton SO17 1BJ, United Kingdom

Received 18 July 2006; received in revised form 23 October 2006; accepted 23 October 2006
Available online 4 December 2006

**Abstract**

Mesoporous manganese dioxide supercapcitor electrode materials were electrochemically deposited onto silicon substrates coated with Pt using triblock copolymer species (Pluronic P123 and F127) as the structure-directing agents. Deposited electrodes of manganese dioxide film were physically characterized by X-ray diffraction (XRD), scanning electron microscopy (SEM) and transmission electron microscopy (TEM), and were electrochemically characterized by cyclic voltammetry (CV) in 0.5 M $Na_2SO_4$ electrolyte. Maximum specific capacitance (SC) values of 449 F $g^{-1}$ was obtained at a scan rate of 10 mV $s^{-1}$ from F127 templated mesoporous $MnO_2$.


*Keywords:* Manganese dioxide; Supercapacitors; Lyotropic liquid crystalline; Electrodeposition

## 1. Introduction

In recent years, electrochemical capacitors or supercapacitors have attracted considerable attention due to their potential applications ranging from mobile devices to electric vehicles [1]. Supercapacitors are basically classified into two types depending on the nature of charge-storage mechanisms [2,3]: (a) the so-called "electrical double-layer capacitors", which exhibit a nonfaradaic reaction with accumulation of charges at the electrode/electrolyte interface; and (b) the so-called redox supercapacitors, which utilize the charge-transfer pseudocapacitance arising from reversible faradaic reactions occurring at the electrode surface.

Many researches in this area have been focused on the development of electrode materials having high specific surface areas. Carbon-based materials have been employed as main electrode materials in electrical double-layer capacitors [4,5]. In the case of redox supercapacitors, various noble and transition metal oxides (e.g. $RuO_2$, $IrO_2$, NiO, $CoO_x$, $MnO_2$, etc.) [6–9] and conducting polymer [10,11] were employed as electrode materials with their charge-storage mechanisms based predominantly on pseudocapacitance. Among these materials, hydrous $RuO_2$ has been found to be most promising and has been extensively studied as it possesses high specific capacitance values ranging from 720 to 760 F $g^{-1}$ [12,13]. However, the high cost and toxic nature of $RuO_2$ limit it from broad applications and have prompted the research interest to focus on other transition metal oxides. In this respect $MnO_2$ is one of the most attractive candidates for supercapacitor electrode materials because of its environmental friendliness, low cost, and favorable pseudocapacitive characteristics [14]. Manganese oxides as pseudocapacitor electrode materials were fabricated via electrochemical and chemical routes. Pang et al. [15] reported the synthesis of $MnO_2$ thin films on nickel foils by electrodeposition and by sol–gel method. Lee et al. synthesized $MnO_2$ by a simple thermal decomposition of ground $KMnO_4$ powder. Prasad et al. [16,17] showed that nanostructured $MnO_2$ and $MnO_2$ based-mixed oxides can be deposited by a potentiodynamic method at a high scan rate. Subramanian et al. [18] reported the synthesis of $MnO_2$ by a hydrothermal route under mild condition. However, comparing with $RuO_2$, $MnO_2$ exhibits lower electrochemical capacitance performance. It is

* Corresponding author. Tel.: +86 931 891 2517; fax: +86 931 891 2582.
*E-mail address:* lihl@lzu.edu.cn (H.-L. Li).

0378-7753/$ – see front matter © 2006 Elsevier B.V. All rights reserved.
doi:10.1016/j.jpowsour.2006.10.100

therefore essential to improve the capacitance performance of $MnO_2$.

The fabrication of nanostructured materials using surfactant mesophases as templates has proved to be a very promising area of research [19–23]. One particularly versatile approach is the use of lyotropic liquid crystalline mesophases of nonionic amphiphilic triblock copolymers acting as a structure-directing agent [24–29]. By using this approach, mesoporous silica and transition metal oxides (e.g. $TiO_2$, $ZrO_2$, $Al_2O_3$, $SnO_2$, etc.) [30,31] with well-defined long-range periodicities have been fabricated. In this paper, we report the electrodeposition of various mesoporous $MnO_2$ on silicon substrates coated with Pt using triblock copolymer species (Pluronic P123 and F127) as the structure-directing agents. The mesoporous nanostructure of $MnO_2$ was characterized using TEM, low angle XRD, and polarized microscope. The electrochemical properties of the mesoporous $MnO_2$ as supercapacitor electrode materials were extensively investigated by the means of cyclic voltammetry.

## 2. Experimental

### 2.1. Chemicals

The triblock copolymer Pluronic P123 ($EO_{20}PO_{70}EO_{20}$) and Pluronic F127 ($EO_{106}PO_{70}EO_{106}$) were purchased from Aldrich and BASF, respectively. The manganese acetate, potassium acetate, sodium sulfate, ethanol (99.9%) and 2-propanol (99%) were obtained from Shanghai Chemical Reagent Co. All chemicals were used as received without further purification and all aqueous solutions were prepared using high purity water (18 MΩ cm).

### 2.2. Preparation of liquid crystalline templates

The electrolyte used in the electrodeposition of mesoporous $MnO_2$ was the binary system of 60 wt% surfactant P123 (or 50 wt% F127) and 40 wt% (or 50 wt%)aqueous solution containing 0.5 M manganese acetate ($MnAc_2$) and 0.51 M potassium acetate (KAc). For mesoporous manganese dioxide deposition, manganese salts aqueous solution was mixed with surfactants to obtain homogeneous liquid crystalline. In liquid crystalline mesophase, anions have great influence on the hydrophilicity of nonionic surfactants [32,33], so manganese acetate was selected for electrolyte solution. The liquid crystalline phase mixture was sealed in a capped vial and allowed to stand in a thermostated oven at 40 °C for 30 min, which was followed by vigorous stirring with a glass rod. This heating/mixing process was repeated at least three times to achieve homogeneity.

### 2.3. Electrodeposition

The electrochemical deposition was conducted on a CHI440a electrochemical workstation (Chenhua, Shanghai), by using a conventional three-electrode system composed of a 1 $cm^2$ platinum/silicon (Pt/Si) working electrode, a large surface area platinum counter electrode, and a standard saturated calomel reference electrode (SCE). The electrodeposition was carried out at 1.0 V versus SCE at room temperature to give a totally passed charge of 0.5 C for the same required amount of $MnO_2$.

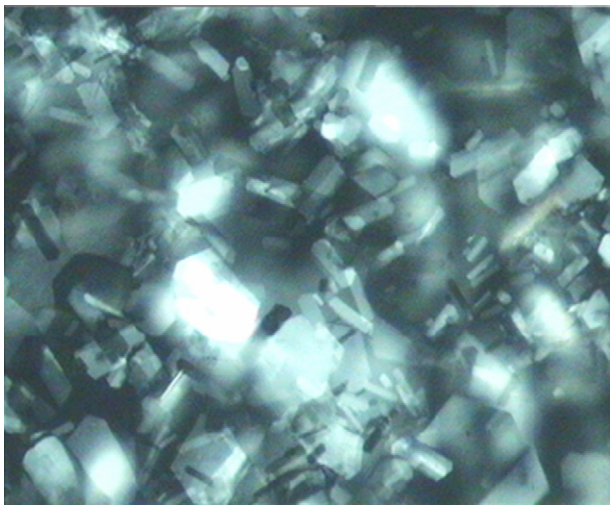

Fig. 1. Polarized optical microscopy (POM) image for binary system of a hexagonal $MnAC_2$:P123 liquid crystalline phase.

After deposition the working electrode was immersed in 2-propanol for 24 h which was regularly replaced every 2 h to remove the surfactant, and then rinsed in high purity water and dried in ambient air. The film was then heat-treated at 200 °C for 2 h.

### 2.4. Characterization

The phase behavior was investigated by polarized optical microscopy (POM, XPF-330, Caikang, Shanghai) equipped with a KEL-XMT-3100 heating stage and temperature control unit. Thin films of the liquid crystalline were prepared by sandwiching the mixture between a glass slide and cover slip. X-ray diffraction (XRD) patterns were recorded on a Bruker D8 Advance diffractometer with Cu Kα as the radiation source (λ = 0.154 nm). Scanning electron microscopy (SEM) was carried out with a Quanta 2000 microscope operated at 20 kV for morphology of manganese dioxide film on substrate. Transmission electron microscopy (TEM) was carried out with FEI Tecnai $G^2$ 20 S-TWIN microscopes operated at 200 kV. The electrochemical measurements of the samples were performed on CHI440a electrochemical workstation.

## 3. Results and discussion

### 3.1. Phase characterization

Since the final nanostructure of mesoporous films was determined by the structure of lyotropic liquid crystalline phase used, it is important to characterize the phase structure of liquid crystalline before deposition. Fig. 1 shows a typical POM image of liquid crystalline mixture containing 60 wt% P123 and 40 wt% aqueous solution. The characteristic texture is not a clear indication of the hexagonal structure. [35] However, the phase structure of liquid crystalline mixtures was also identified by low-angle

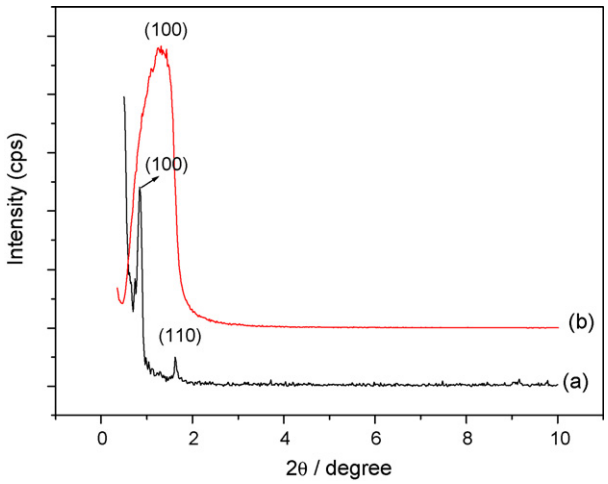


Fig. 2. Low-angle XRD pattern of (a) $MnAc_2$:P123 liquid crystalline and (b) manganese dioxide deposited from (a) on Pt/Si substrate.

XRD. Fig. 2a shows the low angle XRD pattern of the liquid crystalline templating mixture from P123. As can be seen that the liquid crystalline templating mixture exhibits two well-resolved diffraction peaks with *d*-spacings of 103.8 and 54.3 Å, respectively. These *d*-spacings are close to the ratio $1:1/\sqrt{3}$, and are consistent with the (1 0 0) and (1 1 0) diffraction planes of the hexagonal structures.

The liquid crystalline mixture containing 50 wt% F127 and 50 wt% electrolyte has no optical texture under POM, indicating that the mixture is cubic phase because cubic phases are all optically isotropic. It was found that the mixture from F127 is more viscous than that from P123. The liquid crystalline templating mixture from F127 (Fig. 3a) exhibits one peak with *d*-spacing of 124.0 Å, which can be indexed as (1 1 0) diffraction plane of the cubic structure [34].

### 3.2. Structure characterization (SEM, TEM and XRD)

Low-angle XRD patterns for the corresponding mesoporous manganese dioxide films are shown in Figs. 2b and 3b. A strong

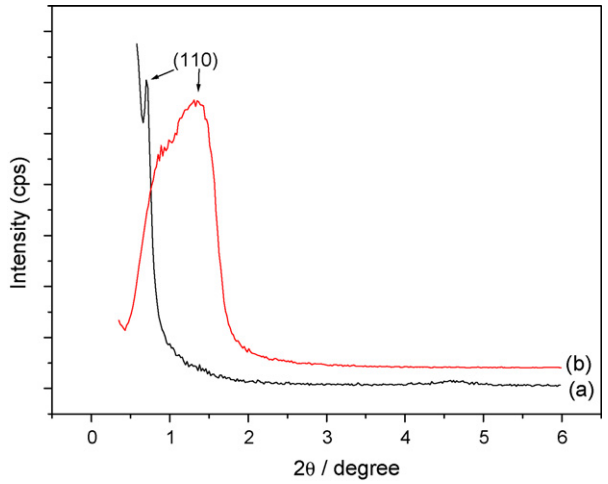


Fig. 3. Low-angle XRD pattern of (a) $MnAc_2$:F127 liquid crystalline and (b) manganese dioxide deposited from (a) on Pt/Si substrate.

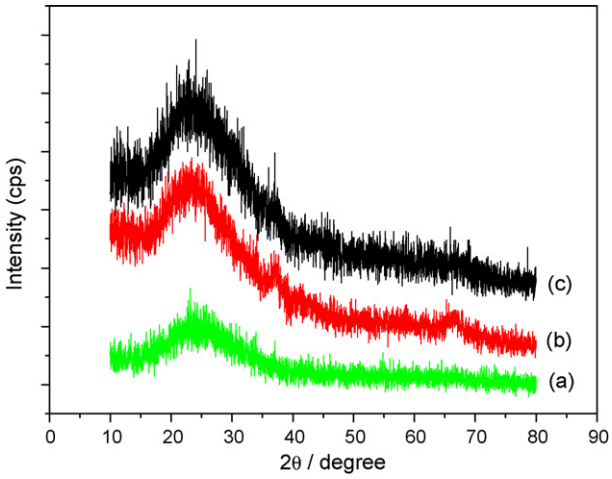


Fig. 4. Wide-angle XRD patterns of (a) glass substrate, (b) F127 and (c) P123 templated manganese dioxide samples, respectively. Samples were heat-treated at 200 °C for 2 h.

reflection peak is observed at $2\theta$ of 1.32° from P123 templated manganese dioxide film (Fig. 2b). The peak is expected to be from $d_{100}$ plane of the hexagonal mesophase structure, corresponding to a *d*-spacing of 6.7 nm and a pore to pore distance of 7.7 nm. F127 templated manganese dioxide film (Fig. 3b) also has one peak which is expected to be from $d_{110}$ plane of the mesostructure with a *d*-spacing of 6.75 and a pore to pore distance of 7.8 nm. Both P123 and F127 templated manganese oxide films show their peaks shift to the smaller *d*-spacing value comparing with corresponding templating mixtures. This result is unexplained and not mentioned in the previous work. The presence of diffraction peak indicates that the ordered mesophase structure in the template is preserved in the deposited film. However, the broadening of the film's diffraction peak compared with that of liquid crystalline mixture and the presence of only a single peak are due to a partial destruction of long-range order during electrodeposition and sequential post-treat. The long-range order can be estimated from the Debye–Sherrer (DS) formula, which gives 6–7 nm for the film and 10–12 nm for the template mixture.

Fig. 4 illustrates the wide-angle XRD patterns of mesoporous $MnO_2$ films templated from P123 (c) and F127 (b). Both the films were heat-treated at 200 °C for 2 h before measurement. The broad peak between $2\theta = 20°$ and 30° is the peak of glass substrate. Peaks at $2\theta = 36.9°$ and 65.7° are obviously observed. It indicated that the crystalline state of the sample contains $MnO_2$ [14]. Lack of clear peaks, low intension and broadening of peaks indicate the amorphous nature and the small size of crystalline grain.

Surface morphologies of different surfactant templated mesoporous $MnO_2$ films are imaged by SEM as shown in Fig. 5. Fig. 5a shows the $MnO_2$ films deposited from P123. After deposition, the surfactant was completely removed from the electrode. The films surface exhibits a copy of lyotropic liquid crystalline template with sponge-like morphology. The surface structure of mesoporous manganese dioxide films deposited from F127 is shown in Fig. 5b, which has cheese-like morphology with porosity. But there is no obvious evidence for

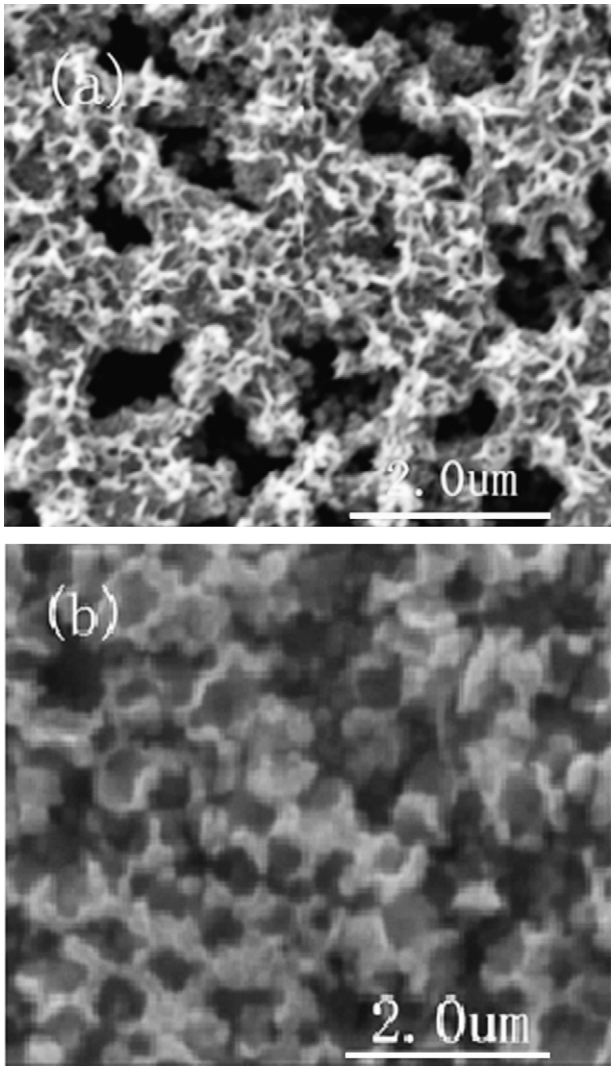


Fig. 5. Scanning electron microscopy (SEM) of (a) P123 and (b) F127 templated manganese dioxide films on Pt/Si substrate. Manganese dioxide was treated at 200 °C for 2 h.

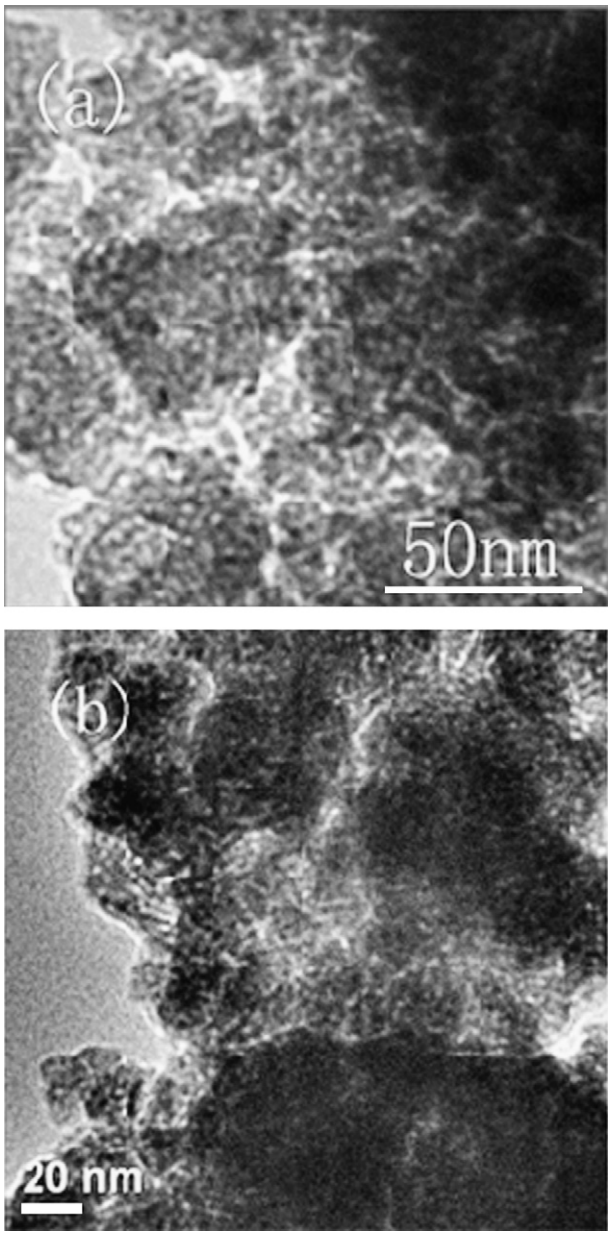


Fig. 6. Transmission electron microscopy (TEM) of (a) P123 and (b) F127 templated manganese dioxide. Manganese dioxide was treated at 200 °C for 2 h.

mesostructure visible on SEM. To examine the nanostructure of the electrodeposited manganese dioxide films, it is necessary to use TEM.

Fig. 6 shows the TEM images of mesoporous $MnO_2$ films that electrodeposited from F127 (b) and P123 (a) liquid crystalline template. The light regions correspond to pore left after removal of the surfactant template from the electrodeposited film and the dark areas are the electrodeposited manganese dioxide materials. TEM images show a less ordered mesoporous structure, which are consistent with only one peak appearing in low-angle XRD patterns, but the films are uniform and homogeneous. The pore diameter observed from TEM is about 4 nm. The disorder of the films may be due to the reaction complexity during cathodic electrodeposition of $MnO_2$ films [35] and heat-treated process which results in pore structure defects and pore size contraction. The contraction is also often caused by complete removal of the surfactant and further condensation of the network [36].

### 3.3. Electrochemical characterization

Cyclic voltammetry (CV) was used to investigate the capacitor behavior of the mesoporous $MnO_2$ films. Fig. 7 shows the CV of $MnO_2$ films deposited from $MnAC_2$ aqueous solution (a), F127 (b) and P123 (c) liquid crystalline templates at a scan rate of 100 mV $s^{-1}$ in 0.5 M $Na_2SO_4$ aqueous solution. In these figures, no obvious redox peak is found. The specific capacitance values calculated from the CV curves were 88, 246 and 212 F $g^{-1}$ for nonporous, F127 templated, and P123 templated $MnO_2$ films, respectively. For calculating the specific capacitance from CV curves, the mass of material is estimated by Faraday law on the assumption that faraday current efficiency for deposition is 100%, and the total capacitance for electrochemical deposition is 0.5 C. The electrodeposited $MnO_2$ films directly from aqueous

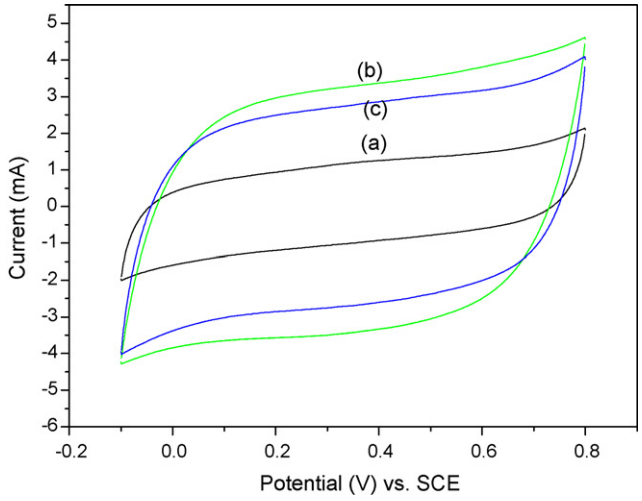


Fig. 7. Cyclic voltammograms of the manganese dioxide deposited from (a) aqueous solution, (b) F127 and (c) P123 liquid crystalline templates in 0.5 M $Na_2SO_4$ solution at RT with a potential scan rate of 100 mV $s^{-1}$.

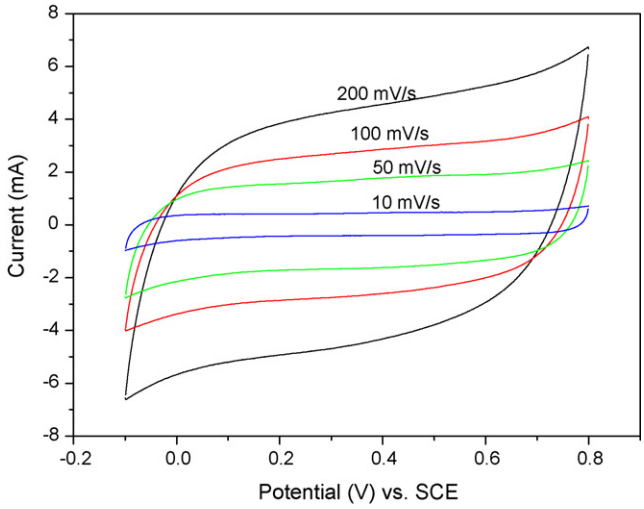


Fig. 9. Cyclic voltammograms of the manganese dioxide deposited from P123 liquid crystalline templates in 0.5 M $Na_2SO_4$ solution at RT with different potential scan rate.

solution showed the lowest specific capacitance, a tendency to delaminate from the substrate, and were easily destroyed at low scan rate or in galvanostatic charge–discharge procedure to compare with those obtained from surfactant templates.

Fig. 8 shows the CV curves of $MnO_2$ deposited from F127 template measured at different scan rates of 200, 100, 50 and 10 mV $s^{-1}$, and the specific capacitance values were found to be 192, 248, 320, 449 F $g^{-1}$, respectively. The CV curves of $MnO_2$ deposited from P123 template at different scan rates were showed in Fig. 9. The specific capacitance values were estimated to be 167, 212, 273 and 377 F $g^{-1}$ corresponding to the scan rates of 200, 100, 50 and 10 mV $s^{-1}$. The CV curves obtained at different scan rate show roughly rectangular mirror images with respect to the zero-current line [37] and symmetric *I–E* responses, indicating the fact that Faraday redox reactions are highly electrochemically reversible. The shape of voltammetric curves is not significantly influenced by the scan rate of CV, and over most of potential range the current is a constant at corresponding scan rate. This result indicates that $MnO_2$ film electrodes prepared by electrodeposited from surfactant templates show a nature of ideally capacitive characteristic.

Fig. 10 shows the charge–discharge behavior of the electrodeposited $MnO_2$ films from F127 and P123 liquid crystalline template. The typical result was measured from −0.1 to 0.8 V versus SCE in 0.5 mol $L^{-1}$ $Na_2SO_4$ at the current density of 1 mA $cm^{-1}$. As shown in Fig. 10, the charge curves are very symmetric to the corresponding discharge counterparts in the whole potential region and the slope of curves is potential independent and maintains the constant value at corresponding current density. The result also indicates the mesoporous $MnO_2$ films have the ideal capacitive behaviors for electrochemical capacitors.

The difference of specific capacitance obtained from P123 and F127 may be due to the pore accessibility in the mesoporous films. The mesoporous film obtained from F127 is expected

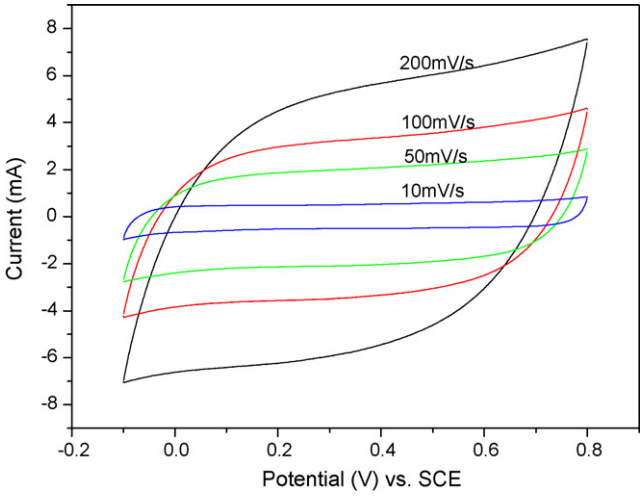


Fig. 8. Cyclic voltammograms of the manganese dioxide deposited from F127 liquid crystalline templates in 0.5 M $Na_2SO_4$ solution at RT with different potential scan rate.

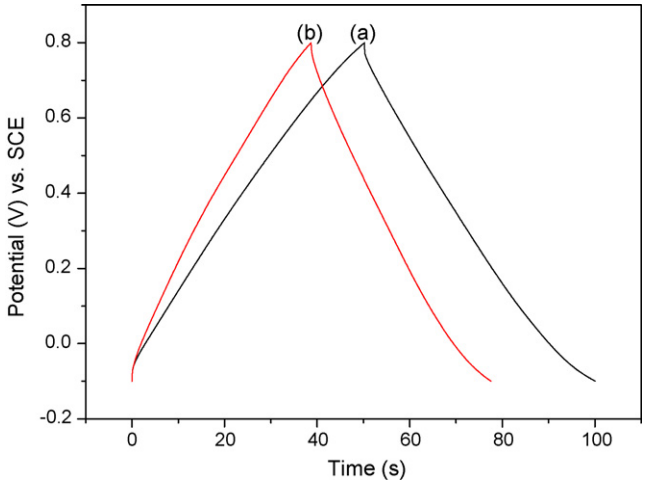


Fig. 10. Galvanostatic charge–discharge cycling in 0.5 M $Na_2SO_4$ for thin films of manganese dioxide deposited from (a) F127 and (b) P123 liquid crystalline templates.

to have bicontinuous 3D mesoporous network structure, which may result in enhanced pore accessibility, and thus the higher specific capacitance. Both the mesoporous films obtained from P123 and F127 exhibit higher specific capacitance than that of nonporous film. The above results demonstrate that mesoporous $MnO_2$ film electrode is a good candidate for an electrochemical capacitor.

## 4. Conclusion

In the present work, we present a novel methodology for electrodeposition of mesoporous $MnO_2$ films from lyotropic liquid crystalline phases Pluronic surfactants. Our results obtained from TEM and low angle XRD indicated the presence of a nanostructure and support a direct templating mechanism for the electrodeposition of mesoporous $MnO_2$ films. The CV studies show that the mesoporous films exhibit higher specific capacitance than nonporous film, which attribute to a larger effective surface area within mesoporous films. In addition, the charge–discharge cycling tests show that the mesoporous $MnO_2$ films exhibit a good cycle profile. This new templating approach will have potential application to fabricate supercapacitor materials.

## Acknowledgment

This work is supported by the National Nature Science Foundation of China (NNSFC60471014).

## References

[1] B.E. Conway, Electrochemical Supercapacitors, Kluwer Academic Publishers, New York, 1999.
[2] B.E. Conway, J. Electrochem. Soc. 138 (1991) 1539.
[3] S. Sarangapani, B.V. Tilak, C.P. Chen, J. Electrochem. Soc. 143 (1996) 3791.
[4] E. Frackowiak, F. Béguin, Carbon 39 (2001) 937.
[5] C. Lin, B.N. Popov, H.J. Ploehn, J. Electrochem. Soc. 149 (2002) A167.
[6] J.P. Zheng, P.J. Cygan, T.R. Jow, J. Electrochem. Soc. 142 (1995) 2699.
[7] A.A.F. Grupioni, E. Arashiro, T.A.F. Lassali, Electrochim. Acta 48 (2002) 407.
[8] C. Lin, J.A. Ritter, B.N. Popov, J. Electrochem. Soc. 145 (1998) 4097.
[9] V. Srinivasan, J.W. Weidner, J. Electrochem. Soc. 147 (2000) 880.
[10] A. Rudge, J. Davey, I. Raistrick, S. Gottesfeld, J. Power Sources 47 (1994) 89.
[11] A. Rudge, J. Davey, I. Raistrick, S. Gottesfeld, Electrochim. Acta 39 (1994) 273.
[12] J.P. Zheng, T.R. Jow, J. Electrochem. Soc. 144 (2026) (1997).
[13] J.P. Zheng, T.R. Jow, Electrochem. Solid-State Lett. 2 (1999) 359.
[14] R.N. Reddy, R.G. Reddy, J. Power Sources 124 (2003) 330.
[15] S.C. Pang, M.A. Anderson, T.W. Chapman, J. Electrochem. Soc. 147 (2000) 444.
[16] K.R. Prasad, N. Miura, J. Power Sources 135 (2004) 354.
[17] K.R. Prasad, N. Miura, Electrochem. Commun. 6 (1004) (2004).
[18] V. Subramanian, H. Zhu, B. Wei, J. Power Sources 159 (2006) 361.
[19] C.G. Goltner, S. Henke, M.C. Weissenberger, M. Antonietti, Angew. Chem. Int. Ed. Engl. 37 (1998) 613.
[20] I. Honma, H.S. Zhou, D. Kundu, A. Endo, Adv. Mater. 12 (2000) 1529.
[21] C.G. Göltner, B. Berton, E. Kramer, M. Antonietti, Adv. Mater. 11 (1999) 395.
[22] F. Schuth, Chem. Mater. 13 (2001) 3184.
[23] T.M. Dellinger, P.V. Braun, Chem. Mater. 16 (2004) 2201.
[24] P.C.A. Alberius, K.L. Frindell, R.C. Hayward, E.J. Kramer, G.D. Stucky, B.F. Chmelka, Chem. Mater. 14 (2002) 3284.
[25] D. Zhao, P.D. Yang, N. Melosh, Y.L. Feng, B.F. Chmelka, G. Stucky, Adv. Mater. 10 (1998) 1380.
[26] N.A. Melosh, P. Davidson, B.F. Chmelka, J. Am. Chem. Soc. 122 (2000) 823.
[27] P. Feng, X. Bu, G.D. Stucky, D.J. Pine, J. Am. Chem. Soc. 122 (2000) 994.
[28] P. Feng, X. Bu, D.J. Pine, Langmuir 16 (2000) 5304.
[29] L. Wang, X. Chen, J. Zhan, Y. Chai, C. Yang, L. Xu, W. Zhuang, B. Jing, J. Phys Chem. B 109 (2005) 3189.
[30] P. Yang, D. Zhao, D.I. Margolese, B.F. Chmelka, G.D. Stucky, Chem. Mater. 11 (2813) (1999).
[31] P. Yang, D. Zhao, D.I. Margolese, B.F. Chmelka, G.D. Stucky, Nature 396 (1998) 152.
[32] O. Dag, S. Alayoglu, C. Tura, O. Celik, Chem. Mater. 15 (2711) (2003).
[33] O. Dag, S. Alayoglu, I. Uysal, J. Phys. Chem. B 108 (2004) 8439.
[34] G. Wanka, H. Hoffmann, W. Ulbricht, Macromolecules 27 (1994) 4145.
[35] S. Rodrigues, N. Munichandraiah, A.K. Shukla, J. Appl. Electrochem. 28 (1998) 1235.
[36] N. Husing, B. Launay, D. Doshi, G. Kickelbick, Chem. Mater. 14 (2002) 2429.
[37] N. Nagarajan, H. Humadi, I. Zhitomirsky, Electrochim. Acta 51 (2006) 3039.